Simultaneous imaging of local calcium and single sarcomere length in rat neonatal cardiomyocytes using yellow Cameleon-Nano140

Seiichi Tsukamoto,[1]* Teruyuki Fujii,[1]* Kotaro Oyama,[1]* Seine A. Shintani,[2] Togo Shimozawa,[3] Fuyu Kobirumaki-Shimozawa,[1] Shin'ichi Ishiwata,[4] and Norio Fukuda[1]

[1]Department of Cell Physiology, The Jikei University School of Medicine, Minato-ku, Tokyo 105-8461, Japan
[2]Department of Physics, Graduate School of Science, The University of Tokyo, Bunkyo-ku, Tokyo 113-0033, Japan
[3]Department of Life Science and Medical Bioscience, School of Advanced Science and Engineering, Waseda University, Sinjuku-ku, Tokyo 162-8480, Japan
[4]Department of Physics, Faculty of Science and Engineering, Waseda University, Shinjuku-ku, Tokyo 169-8555, Japan

In cardiac muscle, contraction is triggered by sarcolemmal depolarization, resulting in an intracellular Ca^{2+} transient, binding of Ca^{2+} to troponin, and subsequent cross-bridge formation (excitation–contraction [EC] coupling). Here, we develop a novel experimental system for simultaneous nano-imaging of intracellular Ca^{2+} dynamics and single sarcomere length (SL) in rat neonatal cardiomyocytes. We achieve this by expressing a fluorescence resonance energy transfer (FRET)–based Ca^{2+} sensor yellow Cameleon–Nano (YC-Nano) fused to α-actinin in order to localize to the Z disks. We find that, among four different YC-Nanos, α-actinin–YC-Nano140 is best suited for high-precision analysis of EC coupling and α-actinin–YC-Nano140 enables quantitative analyses of intracellular calcium transients and sarcomere dynamics at low and high temperatures, during spontaneous beating and with electrical stimulation. We use this tool to show that calcium transients are synchronized along the length of a myofibril. However, the averaging of SL along myofibrils causes a marked underestimate (~50%) of the magnitude of displacement because of the different timing of individual SL changes, regardless of the absence or presence of positive inotropy (via β-adrenergic stimulation or enhanced actomyosin interaction). Finally, we find that β-adrenergic stimulation with 50 nM isoproterenol accelerated Ca^{2+} dynamics, in association with an approximately twofold increase in sarcomere lengthening velocity. We conclude that our experimental system has a broad range of potential applications for the unveiling molecular mechanisms of EC coupling in cardiomyocytes at the single sarcomere level.

The Journal of General Physiology

INTRODUCTION

In mammals, Ca^{2+} plays a critical role as a second messenger in various physiological functions. It is widely recognized that recent advances in optical fluorescence technologies have revealed that, in various types of mammalian cells, the intracellular Ca^{2+} concentration ($[Ca^{2+}]_i$) does not increase homogeneously, but rather heterogeneously, and the heterogeneous increase in $[Ca^{2+}]_i$ and the ensuing diffusion of Ca^{2+} in the cytosolic space play a key role in exerting unique cellular functions, such as Ca^{2+} sparks that occur at/around the T tubules in cardiac (e.g., Bers, 2001, 2002; Prosser et al., 2010) or skeletal (e.g., Ríos et al., 1999; González et al., 2000) muscle cells. Therefore, it is imperative to develop an experimental system in which local $[Ca^{2+}]_i$ and the position of subcellular structures, molecular complexes, or molecules can be simultaneously measured in the cytosolic μm-domain at high spatial and temporal resolution for fully understanding the physiology of various cellular functions at the molecular level.

In cardiac muscle, the thin filament state is regulated by a change in $[Ca^{2+}]_i$ on a graded basis, regardless of the development stage (see Bers, 2001, 2002; Colella et al., 2008; Prosser et al., 2010; Kobirumaki-Shimozawa et al., 2014; and references therein). Likewise, cardiac contractility is highly dependent on sarcomere length (SL); indeed, a change of merely ~100 nm causes a dramatic change in contractile performance (known as the Frank-Starling relation; see e.g., Allen and Kentish, 1985; Katz, 2002; Hanft et al., 2008; Fukuda et al., 2010; Kobirumaki-Shimozawa et al., 2014; and references therein). This intrinsic nature of the cardiac contractile system requires an accurate measurement of SL to enhance our understanding of myocardial dynamic behaviors at the molecular level, not only in adults but also in neonates whose cardiomyocytes undergo rapid growth for normal heart development via biochemical/paracrine and mechanical signaling (see Jacot et al.,

*S. Tsukamoto, T. Fujii, and K. Oyama contributed equally to this paper.
Correspondence to Norio Fukuda: noriof@jikei.ac.jp

Abbreviations used: $[Ca^{2+}]_i$, intracellular Ca^{2+} concentration; CaM, calmodulin; CaT, Ca^{2+} transient; EC, excitation–contraction; EMCCD, electron-multiplying charge-coupled device; FFT, fast-Fourier transform; F.I., fluorescence intensity; fps, frames per second; FRET, fluorescence resonance energy transfer; Iono, ionomycin; ISO, isoproterenol; OM, omecamtiv mecarbil; PLN, phospholamban; SL, sarcomere length; TnI, troponin I; YC-Nano, yellow Cameleon–Nano.

The Rockefeller University Press $30.00
J. Gen. Physiol. 2016 Vol. 148 No. 4 341–355
www.jgp.org/cgi/doi/10.1085/jgp.201611604

2008, 2010; Rodriguez et al., 2011; and references therein). In a previous study, by expressing α-actinin–AcGFP in sarcomeric Z disks, we analyzed sarcomere dynamics in cardiomyocytes (Shintani et al., 2014). We demonstrated clearly that the averaging of the lengths of sarcomeres along the myocyte caused marked underestimation of sarcomere lengthening speed caused by the superpositioning of different timings for lengthening between sequentially connecting sarcomeres along myofibrils. This finding emphasizes the importance of investigation on how the individual, multiple behaviors of cardiac sarcomeres are integrated to yield overall cellular functions, by taking advantage of advanced nanoscale analyses. More recently, we demonstrated in the beating heart in living mice that the sarcomere dynamics, rather than the initial SL per se, determines the magnitude of ventricular contractility (Kobirumaki-Shimozawa et al., 2016). Although our experimental system using cultured myocytes in the previous experiments enables nano-imaging of single sarcomere dynamics (i.e., SD, 3 and 8 nm in the absence and presence of the Ca^{2+} indicator Fluo-4, respectively, at 50 frames per second [fps]) simultaneous with $[Ca^{2+}]_i$ changes, the heterogeneity of changes in $[Ca^{2+}]_i$ in the myocyte, caused by, e.g., Ca^{2+} sparks and/or waves, cannot be obtained at high spatial resolution, and the dynamics of a single sarcomere in a particular region of a myocyte needs to be analyzed in relation to the mean $[Ca^{2+}]_i$. Therefore, simultaneous, high-precision measurements of Z disk spacings and local $[Ca^{2+}]_i$ in localized, specific regions of living cardiomyocytes is essential to elucidate the mechanism by which the cellular excitation–contraction (EC) coupling is tuned via Ca^{2+}-dependent dynamics of sequentially connecting sarcomeres.

Since the development of Quin 2 by Tsien and colleagues for the visualization of cytosolic Ca^{2+} (first applied in intact lymphocytes; see Tsien, 1980; Tsien et al., 1982a,b), various small molecule Ca^{2+} indicators with differing K_d values (e.g., Fura-2, Fluo-3, Fluo-4, and Fluo-8) have been developed and indeed applied for cardiac physiology investigations in various specimens under varying conditions (see Bers, 2001; and references therein). By using these Ca^{2+} indicators, local Ca^{2+} gradients within specific subregions of individual sarcomeres have been detected (Hollingworth et al., 2000; Zoghbi et al., 2000; Previs et al., 2015). However, as demonstrated by Tanaka et al. (2002), these Ca^{2+} indicators are introduced into cardiomyocytes in isolated perfused hearts at a lesser magnitude as the solution temperature increases (from ∼25°C), casting possible limitations for experimentations at physiologically relevant temperatures and above.

To solve the issues associated with small molecule Ca^{2+} indicators, recent molecular biology technologies have allowed for the analyses of changes in $[Ca^{2+}]_i$ by genetically expressing Ca^{2+}-sensitive fluorescent proteins inside cells. In particular, Tallini et al. (2006) ubiquitously expressed GCaMP2 in cardiomyocytes and successfully visualized Ca^{2+} movements in the surface of the beating heart in living rats (at 128 fps). Likewise, the expression of GCaMP6f in junctional proteins (i.e., triadin1 and junctin) revealed "junctional Ca^{2+} transients" (i.e., Ca^{2+} nano-sparks) in rat cardiomyocytes (Shang et al., 2014). However, by varying the levels of background $[Ca^{2+}]_i$, even at rest, the use of GCaMP-like Ca^{2+}-sensitive fluorescent proteins may have fundamental limitations in the accurate analysis of local $[Ca^{2+}]_i$ in cardiomyocytes in relation to SL dynamics in the region.

Cameleon was genetically engineered based on green fluorescent protein (GFP) for visualization of $[Ca^{2+}]_i$ in living cells by Miyawaki et al. (Miyawaki et al., 1997, 1999), and it enables ratiometric measurements of $[Ca^{2+}]_i$ in living cells. This ratiometric measurement enables high precision quantification of changes in $[Ca^{2+}]_i$, regardless of the level of background $[Ca^{2+}]_i$. Upon Ca^{2+}-binding to its calmodulin (CaM) element, Cameleon undergoes a conformation change and radiates an altered wavelength (as depicted in Fig. 1, A and B). Various ultrasensitive Cameleons with differing Ca^{2+}-binding affinities (e.g., yellow Cameleon–Nano [YC-Nano15], YC-Nano50, YC-Nano65, and YC-Nano140) have been engineered (Horikawa et al., 2010), and they are widely used for investigation of $[Ca^{2+}]_i$ in various physiology/cell biology fields.

In the present study, we developed a novel experimental system for real-time simultaneous measurements of sarcomere dynamics and local $[Ca^{2+}]_i$ via expression of various YC-Nanos (YC-Nano15, YC-Nano50, YC-Nano65, and YC-Nano140) in the Z disks in cultured neonatal cardiomyocytes. Our results show that α-actinin–YC-Nano140 is best suited for simultaneous analysis of changes in local $[Ca^{2+}]_i$ and SL dynamics during spontaneous beating, with or without pharmacological perturbations (via β-adrenergic stimulation with isoproterenol [ISO] or enhanced actomyosin interaction with omecamtiv mecarbil [OM]), and at a physiologically relevant frequency of 5 Hz. Physiological implications are discussed.

MATERIALS AND METHODS

This study was performed in accordance with the Guidelines on Animal Experimentation of The Jikei University School of Medicine (Tokyo, Japan). The study protocol was approved by the Animal Care Committee of The Jikei University School of Medicine and the Recombinant Gene Research Safety Committee of The Jikei University School of Medicine.

Expression of α-actinin–YC-Nanos in neonatal cardiomyocytes

Various YC-Nano cDNAs were inherited from the developer K. Horikawa (Tokushima University, Tokushima,

Japan; Horikawa et al., 2010), whereas the α-actinin–AcGFP expression vector was constructed based on our published procedure (Shintani et al., 2014). The expression vector of the α-actinin–YC-Nano (pAct-YCN) was constructed via replacement of AcGFP with YC-Nano (YC-Nano15, YC-Nano50, YC-Nano65, or YC-Nano140) cDNA (Fig. 1 A), and the sequence of the α-actinin–YC-Nano gene was confirmed by dideoxy DNA sequencing on a 3100-Avant Genetic Analyzer (Thermo Fisher Scientific).

Throughout the present study, neonatal cardiomyocytes, rather than adult cardiomyocytes, were used for the following reasons: (a) plasmid transfection is relatively easy and (b) high precision analysis of SL displacement can be achieved without the use of a confocal system (see Shintani et al., 2014). The primary cultured ventricular myocytes of neonatal Wistar rats (1 d) were obtained based on our published protocol (Shintani et al., 2014). The cardiomyocytes were cultured on a glass dish (AGC Techno Glass Co.) coated with collagen (Cellmatrix Type I-C; Nitta Gelatin Inc.) in Dulbecco's Modified Eagle's Medium (Nissui Pharmaceutical Co.) containing 2 mM L-glutamine (Sigma-Aldrich), 10% FBS, 100 U/ml penicillin, and 100 µg/ml streptomycin under the normal cell culture conditions (37°C with 5% CO_2). FBS, penicillin, and streptomycin were purchased from Thermo Fisher Scientific. After 4–5 d, the α-actinin–YC-Nano plasmid was transfected into the cardiomyocytes by using Lipofectamine LTX (Thermo Fisher Scientific), and the cardiomyocytes were observed 1 d after the transfection. Accordingly, an α-actinin–YC-Nano was fused into sarcomeric Z disks (as illustrated in Fig. 1 B; see Results and discussion for details).

Microscopic system

Real-time fluorescence imaging was performed using an inverted optical microscope (IX-70; Olympus) equipped with an electron-multiplying charge-coupled device (EMCCD) camera (iXon3; Andor Technology Ltd.) using a 60× oil immersion objective lens (PlanApo N 60×/1.45 oil; Olympus) or a 100× oil immersion objective lens (UApo N 100×/1.49 oil; Olympus; Fig. S1 B). We observed cardiomyocytes expressing an α-actinin–YC-Nano in 1.5 or 2.0 mM Ca^{2+}-HEPES–Tyrode's solution (see Fukuda et al. [2001] for solution composition) at 22 or 37°C. The temperature was strictly adjusted by a thermostatically controlled incubator on the sample stage (INUG2-ONICS; Tokai Hit Co.). Myocytes were excited by a mercury lamp (Olympus) with an excitation filter (FF01-438/24; Semrock Inc.) and a dichroic mirror (FF458-Di01; Semrock Inc.) as illustrated in Fig. 1 C. For ratiometric imaging of α-actinin–YC-Nanos in the Z disks, a dichroic mirror (FF509-FDi01; Semrock Inc.) and two different types of emission filters (FF01-483/32 and FF01-542/27; Semrock Inc.) were incorporated into the optics system. The cyan and yellow fluorescence signals were simultaneously recorded by an EMCCD camera. The separated fluorescence signals were adjusted by the lens placed in the light path and finally projected in the EMCCD camera (Fig. 1 C). The images were recorded at 33 fps.

For confocal imaging, an inverted optical microscope (IX-73; Olympus) combined with a Nipkow confocal scanner (CSU-X1; Yokogawa Electric Corporation) and an EMCCD camera (iXon Ultra; Andor Technology Ltd.) were used. We used a 100× oil immersion objective lens (UApo N 100×/1.49 oil; Olympus) in this experimentation. Cardiomyocytes were excited by a 488-nm laser light (Vortran Laser Technology, Inc.) or a 561-nm laser light (Cobolt AB). We used a dichroic mirror (Di01-T405/488/561; Semrock Inc.) and an emission filter (YOKO-FF01-520/35 [for 488 nm; Semrock Inc.] or YOKO-FF01-617/73 [for 561 nm; Semrock Inc.]).

Experimental procedures

For Ca^{2+} imaging with Fluo-4, α-actinin–YC-Nano140–expressing cardiomyocytes were preincubated in 1.5 mM Ca^{2+}-HEPES–Tyrode's solution containing 2 µM Fluo-4-AM (Dojindo) for 20 min at 25°C. The changes in $[Ca^{2+}]_i$ during spontaneous beating were analyzed in 1.5 (or 2.0) mM Ca^{2+}-HEPES–Tyrode's solution, at 22°C and 37°C, according to our published protocol (Shintani et al., 2014, 2015). In experiments with ISO (Tokyo Chemical Industry Co.), ionomycin (Iono; Wako Pure Chemical Industries), or OM (Selleck), ISO was dissolved in Ca^{2+}-free HEPES–Tyrode's solution (0.1 mM), and Iono and OM in DMSO (1 mM), all stored at −20°C. The effects of ISO or Iono on the fluorescence resonance energy transfer (FRET) signals from the Z disks of α-actinin–YC-Nano140-expressing cardiomyocytes were investigated during spontaneous beating in 1.5 mM Ca^{2+}-HEPES–Tyrode's solution at 37°C. In the presence of OM, cardiomyocytes were imaged in 1.8 mM Ca^{2+}-HEPES–Tyrode's solution at 36°C. For experiments with electrical stimulation, α-actinin–YC-Nano140–expressing cardiomyocytes were stimulated at 5 Hz (voltage gradient, ∼20 V/cm; duration, 5 ms) in 1.0 mM Ca^{2+}-HEPES–Tyrode's solution at 37°C with an electronic stimulator (SEN-3301; Nihon Kohden) and an isolator (SS-104J; Nihon Kohden; Shintani et al., 2014).

Data analysis

Fluorescence images and Z disk intensities were obtained by the iQ software (Andor Technology). The intensity profiles were obtained by ImageJ software (National Institutes of Health) and analyzed by using a custom-made Excel macro (Microsoft; see Shintani et al. [2014] for details). SL nanometry was performed as described in detail in our previous work (Shintani et al., 2014, 2015). Namely, line profiles of sarcomeres along

myofibrils were obtained by ImageJ (width of line, 5 and 8 pixels [i.e., ∼1.3 and ∼1.2 µm] for 60× and 100× objective lenses, respectively) using yellow fluorescence images. Then, the line profiles were spatially averaged with double-sided pixels (total 3 pixels), and the averaged fluorescence profile at the peak and double-sided 2 pixels (total 5 pixels) was fitted for a single Gaussian function to determine the peak position. For the FRET analyses of the Z disks, fluorescence intensities (F.I.s) at the peak and double-sided pixels (total 3 pixels) were averaged. For the FRET analyses of single cells, the F.I.s in the center of cells (∼130 μm^2) were measured. Background intensity at the area in the absence of cells was subtracted in the FRET analysis.

The minimum and maximum FRET signals (the ratio of yellow fluorescence [F_{yellow}] to cyan fluorescence [F_{cyan}]; F_{yellow}/F_{cyan} denoted by "R") during spontaneous beating were defined as R_0 and R_{max}, respectively. To avoid photobleaching effects, the analyses were performed within 5 s from the start of the observation. For the analysis of a Ca^{2+} transient (CaT) during spontaneous beating, the decay time (that appeared after the peak signal) was defined as the time from 75% to 25% of F_{yellow}/F_{cyan} (e.g., Asahi et al., 2004). The fast-Fourier transform (FFT) analysis was performed by using the OriginPro2015 software (OriginLab Co.) with a rectangular window function in the program.

Immunostaining

For costaining of α-actinin and actin filaments (F-actin), or staining F-actin only, cardiomyocytes were fixed in PBS (Wako Pure Chemical Industries) containing 4% paraformaldehyde for 10 min and incubated in PBS containing 0.1% Triton X-100 (Nacalai Tesque Co.) for 5 min. The fixed cells were washed with PBS and then incubated in blocking solution (PBS containing 1% BSA; Biowest) for 60 min. To stain α-actinin, the cells were incubated in blocking solution containing mouse anti–α-actinin antibody (1:300; monoclonal EA-53; A7811; Sigma-Aldrich) for 60 min; after washing with blocking solution, the cells were incubated in blocking solution containing Alexa Fluor 488–conjugated goat anti–mouse IgG (1:300; A-11001; Thermo Fisher Scientific) for 60 min. To stain F-actin, cardiomyocytes were incubated in blocking solution containing 167 ng/ml tetramethylrhodamine B isothiocyanate–conjugated phalloidin (Sigma-Aldrich) for 20 min.

For costaining of α-actinin and myosin light chain 2 (MLC2v), or staining of MLC2v only, cardiomyocytes were fixed in PBS containing 4% paraformaldehyde for 5 min and then incubated in PBS containing 0.2% Triton X-100 and 4% paraformaldehyde for 10 min. After washing with PBS, the cells were incubated in blocking solution for 60 min. The cells were then incubated in blocking solution containing mouse anti–α-actinin antibody (1:1,000; Sigma-Aldrich) and rabbit anti-MLC2v antibody (1:1,000; 10906-1-AP; Proteintech Group, Inc.), or the anti-MLC2v antibody only, for 60 min. After washing with blocking solution, the cells were incubated in blocking solution containing Alexa Fluor 488–conjugated goat anti–mouse IgG (1:1,000; A-11001; Thermo Fisher Scientific) and Alexa Fluor 594–conjugated donkey anti–rabbit IgG (1:1,000; ab150072; Abcam) or only Alexa Fluor 594–conjugated donkey anti–rabbit IgG for 60 min.

In all cases (i.e., [a] costaining of α-actinin and F-actin, [b] staining of F-actin, [c] costaining of α-actinin and MLC2v, and [d] staining of MLC2v), the cells were visualized in PBS under confocal microscopy after washing with PBS. All experiments were performed at room temperature (∼25°C).

Simulation

We calculated Ca^{2+} binding kinetics of Ca^{2+} indicators using Euler's method in Excel (see Supplemental discussions III and IV and Figs. S4 and S5).

Statistics

Mann-Whitney *U* test and Tukey's test were performed based on the OriginPro2015 software (OriginLab Co.). Statistical significance was assumed to be a p-value of <0.05 (i.e., *, $P < 0.05$; **, $P < 0.01$; ***, $P < 0.001$). NS, not significant ($P > 0.05$). Linear regression analyses were performed in accordance with the method used in our previous studies (e.g., Shintani et al., 2014, 2015).

Online supplemental material

Supplemental discussion I discusses the variance in diastolic SL. Supplemental discussion II discusses the spatial resolution for the SL displacement measurement. Supplemental discussion III discusses the Ca^{2+}-binding properties of Fluo-4 and YC-Nano140. Supplemental discussion IV discusses the apparent increase in diastolic F_{yellow}/F_{cyan} at a stimulation frequency of 5 Hz. Fig. S1 shows fluctuation analyses of the length of a single sarcomere. Fig. S2 shows immunostaining showing localization of α-actinin–YC-Nano140 in the Z disks. Fig. S3 shows a time course of F_{yellow}/F_{cyan} in α-actinin–YC-Nano140–expressing myocytes after treatment with Iono. Fig. S4 shows simulated $[Ca^{2+}]_i$ dynamics with Fluo-4 or α-actinin–YC-Nano140 under spontaneous beating. Fig. S5 shows simulated $[Ca^{2+}]_i$ dynamics with Fluo-4 or YC-Nano140 under electric stimulation at 5 Hz. Video 1 shows a neonatal cardiomyocyte expressed with α-actinin–YC-Nano140 showing spontaneous beating. Video 2 shows neonatal cardiomyocytes expressing various α-actinin–YC-Nanos fused into the Z disks in cardiomyocytes. Video 3 shows a neonatal cardiomyocyte expressing α-actinin–YC-Nano140 showing contractions in response to electric field stimulation. Video 4 shows a neonatal cardiomyocyte expressing α-actinin–YC-Nano140 showing individ-

ual sarcomere dynamics during spontaneous beating. Video 5 shows a neonatal cardiomyocyte expressing α-actinin–YC-Nano140 showing individual sarcomere dynamics and Ca^{2+} waves during spontaneous beating under β-adrenergic stimulation. Video 6 shows a neonatal cardiomyocyte expressing α-actinin–YC-Nano140 showing individual sarcomere dynamics during spontaneous beating under enhanced actomyosin interaction. Table S1 shows a summary of Ca^{2+}-binding parameters of Fluo-4 and YC-Nano140.

RESULTS AND DISCUSSION

First, we expressed α-actinin–YC-Nano140 in the Z disks in neonatal cardiomyocytes, and performed immunofluorescence experiments. Accordingly, immunostaining revealed that (a) the F.I. peaks of α-actinin–YC-Nano140 (or α-actinin) coincided with the centers of F-actin (I-Z-I brush) F.I. signals, and (b) the F.I. peaks of α-actinin–YC-Nano140 (or α-actinin) coincided with the lowest MLC2v (i.e., thick filament) F.I. signal (Fig. S2). These findings support the notion that α-actinin–YC-Nano140 is fused into the Z disks. See Supplemental discussion I.

We then observed local Ca^{2+} and sarcomere dynamics simultaneously in myocytes expressed with α-actinin–YC-Nano140 (i.e., highest K_d [140 nM] among YC-Nanos used in the present study) during spontaneous beating when bathed in HEPES–Tyrode's solution containing 1.5 mM Ca^{2+} at 37°C. Fig. 1 D shows typical fluorescence images of a cardiomyocyte expressing α-actinin–YC-Nano140 during spontaneous beating at the time of peak relaxation (left) or contraction (right; see Video 1). When $[Ca^{2+}]_i$ increases (from "Low" to "High" in Fig. 1 B), Ca^{2+} binds to CaM, which enables CaM to wrap around M13. This conformational change brings Venus and ECFP closer to each other, resulting in an increase in FRET efficiency between them. When excited at 430 nm, YC-Nano140 emits fluorescence of 480 (535) nm in the absence of Ca^{2+} (upon Ca^{2+} binding to CaM), thereby enabling the measurement of local $[Ca^{2+}]_i$ by comparing the fluorescence ratio. Upon change in the state of the myocyte from relaxation to contraction, F_{yellow} increased, whereas F_{cyan} decreased, indicating the occurrence of intracellular CaT triggered via spontaneous depolarization of the sarcolemma. The yellow and cyan fluorescence profiles along myofibrils in Fig. 1 D (as indicated by a yellow rectangle) provide regional $[Ca^{2+}]_i$ and the length of a particular sarcomere, the former of which was obtained by the F_{yellow}/F_{cyan} ratio and the latter by the peak to peak distance between the adjacent Z disks (Fig. 1 E). Because F_{yellow} was higher than F_{cyan} along myofibrils during either relaxation or contraction (compare Fig. 1 D), in the present study, SL was determined by measuring the peak to peak distance of F_{yellow}. Accordingly, the measurement of sarcomere dynamics was enabled simultaneous with changes in $[Ca^{2+}]_i$ in the local domain (Fig. 1, F and G; see kymographs in Fig. 1 F for time-dependent changes in F_{yellow} and F_{cyan}), with a precision of 17 nm (see Supplemental discussion II and Fig. S1 on the precision of SL displacement measurement).

It is worthwhile noting that significant sarcomere lengthening appeared in the first two events in Fig. 1 G in response to a rise in F_{yellow}/F_{cyan}. We consider that this is caused by the effect of contraction of the neighboring sarcomeres along the myofibril (in Fig. 1 D), which pulls sarcomeres in the data trace (hence lengthening detected in response to a rise, not a fall, in $[Ca^{2+}]_i$; as demonstrated in some myocytes expressing α-actinin–AcGFP; see Shintani et al., 2014).

Fig. 2 and Video 2 summarizes the time course of changes in F_{yellow}/F_{cyan} with various α-actinin–YC-Nanos expressed in cardiomyocytes. All α-actinin–YC-Nano constructs (i.e., YC-Nano15, YC-Nano50, YC-Nano65, and YC-Nano140 with K_d values of 15, 50, 65, and 140 nM, respectively) labeled Z disks within 24 h after transfection into cardiomyocytes and enabled detection of F_{yellow}/F_{cyan} changes during spontaneous beating (see individual traces of F_{yellow}/F_{cyan} in Fig. 2 A). α-Actinin–YC-Nano15 (α-actinin–YC-Nano140) exhibited the largest (smallest) values of minimal (R_0) and maximal (R_{max}) FRET signals, with 4.2 ± 0.6 (1.5 ± 0.1) and 4.6 ± 0.6 (2.3 ± 0.3), respectively (Fig. 2 B). The large R_0 and R_{max} values of α-actinin–YC-Nano15 (and the ensuing small ΔR [$=R_{max} - R_0$] and $\Delta R/R_0$ values) indicate that Ca^{2+} binding to α-actinin–YC-Nano15 is nearly saturated even during relaxation; hence, it is unsuitable for the analysis of EC coupling. Accordingly, the change in the FRET signal (ΔR) and the relative change of it ($\Delta R/R_0$) were smallest with α-actinin–YC-Nano15 (ΔR = 0.5 ± 0.2, $\Delta R/R_0$ = 0.1 ± 0.05) and largest with α-actinin–YC-Nano140 (ΔR = 0.8 ± 0.2, $\Delta R/R_0$ = 0.6 ± 0.2; Fig. 2, C and D). It should be noted that for nano-imaging of sarcomere dynamics simultaneous with local $[Ca^{2+}]_i$, high-precision tracings of both F_{yellow} and F_{cyan} from the Z disks are required. In other words, as a principle in the FRET analysis, the farther the F_{yellow}/F_{cyan} ratio is away from 1.0, the more difficult to detect the fluorescence of either cyan or yellow. Indeed, the weak cyan fluorescence of α-actinin–YC-Nano15 made it difficult to analyze the movements of individual sarcomeres from the cyan fluorescence image, even during relaxation. In contrast, α-actinin–YC-Nano140 provided sufficiently detectable fluorescence signals of both cyan and yellow (as in Fig. 1, D–F). Therefore, we concluded that of the α-actinin–YC-Nanos tested, α-actinin–YC-Nano140 was the best suited for the analysis of cardiac EC coupling at the single sarcomere level, and thus we used it in the following experimentations. Likewise, given the fact that $\Delta R/R_0$ can reveal distinct

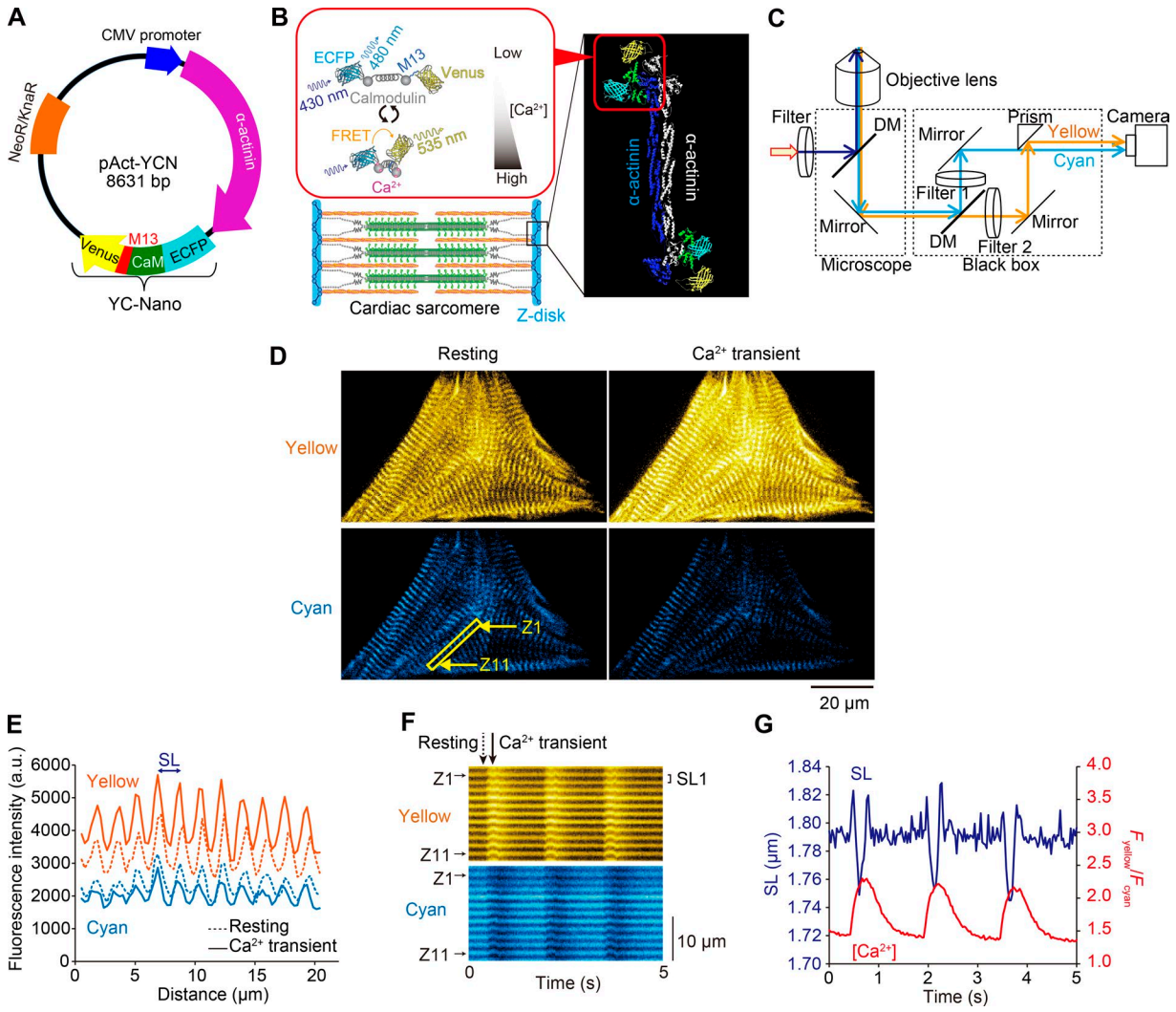

Figure 1. **Expression of α-actinin–YC-Nano140 in sarcomeric Z disks of neonatal cardiomyocytes for simultaneous measurements of local $[Ca^{2+}]_i$ and SL.** (A) Genetic map of pAct-YCN. The plasmid was constructed by modifying pAcGFP-N1 (Takara Bio Inc.). The plasmid encodes α-actinin fused to YC-Nano below the immediate early promoter of CMV ($P_{CMV\ IE}$) and neomycin/kanamycin resistance gene (NeoR/KnaR). (B) Illustration showing the expression of YC-Nano140 in the Z disks and that of a FRET response upon Ca^{2+} binding to CaM. YC-Nano (YC-Nano15, YC-Nano50, YC-Nano65, or YC-Nano140) is composed of ECFP (FRET donor), CaM, CaM-binding peptides (M13), and Venus (FRET acceptor). (C) Schematic of our dual-view fluorescence microscopic system. Yellow and cyan fluorescence signals were separated by dichroic mirrors (DM) and detected simultaneously by an EMCCD camera as a dual view (as in D). Filter 1, 467–499 nm; filter 2, 529–556 nm. Myocytes were excited by violet light (424–450 nm). (D) Epi-illumination images of a spontaneously beating myocyte at the peak of relaxation (left) and contraction (right). Yellow is the FRET acceptor (Venus), and cyan is the FRET donor (ECFP). Note clear F.I. changes for Venus and ECFP upon change in the state of the myocyte; namely, yellow F.I. increases (decreases) while cyan F.I. decreases (increases) during contraction (relaxation). See Video 1. (E) Plot profiles of Venus (yellow) and ECFP (cyan) fluorescence signals along a myofibril in D (shown by a yellow rectangle). SL is determined by the peak to peak distance of F_{yellow}, and the local $[Ca^{2+}]$ change is determined by the FRET signal (i.e., F_{yellow}/F_{cyan}). Dashed and solid lines indicate the signals at rest (D, left) and during CaT (D, right), respectively. (F) Kymographs showing changes in the longitudinal positions of the yellow (top) and cyan (bottom) fluorescence signals. "Z1" and "Z11" indicate the Z disks in the yellow outlined rectangle in D. "SL1" (distance between the peaks of yellow fluorescence) indicates sarcomere #1 along the target myofibril. Dashed and solid arrows indicate the time points at rest and during CaT, respectively, in D and E. (G) Representative graph showing a time-course of changes in F_{yellow}/F_{cyan} (i.e., local $[Ca^{2+}]_i$) and SL in a myocyte showing spontaneous beating at 37°C. Blue, SL; red, F_{yellow}/F_{cyan}. Note that spontaneous beating occurs with a frequency of ∼1.5 Hz in a neonatal rat cardiomyocyte, in that SL shortening (lengthening) starts in response to a rise (fall) in F_{yellow}/F_{cyan} (compare Shintani et al., 2014, 2015). Changes in $[Ca^{2+}]$ were determined by the mean FRET signals (i.e., F_{yellow}/F_{cyan}), and SL, by the mean peak to peak distances of F_{yellow}, along 10 sarcomeres in D (bottom, left).

properties of FRET-based Ca^{2+} signals, at least in the present experimental settings, we used the parameter, rather than ΔR, throughout the present study.

Next, we investigated the rate of rise or fall of the fluorescence signal of α-actinin–YC-Nano140, in comparison with Fluo-4, a commonly used small molecule Ca^{2+}

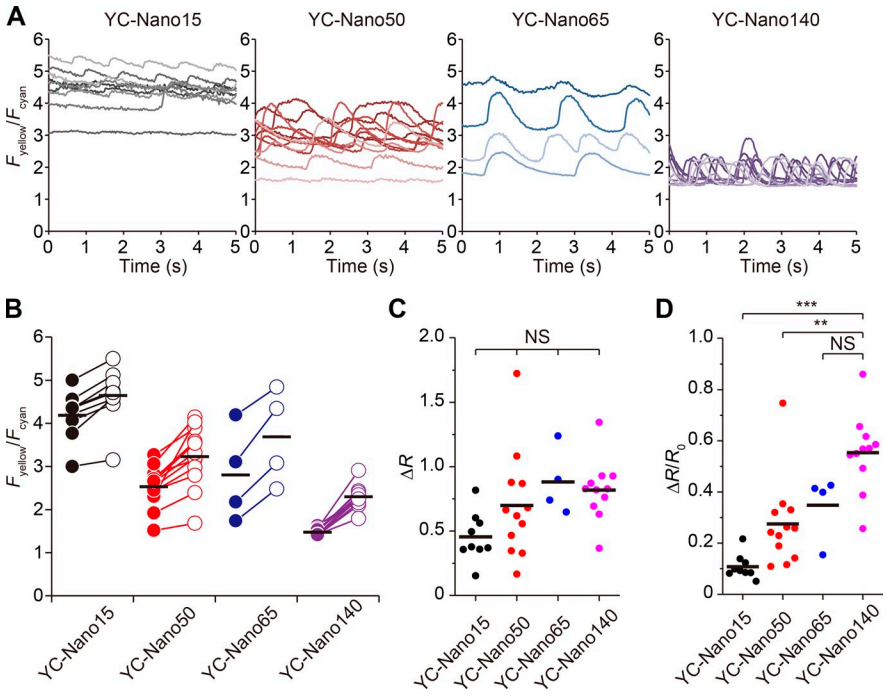

Figure 2. **Time course of FRET signals of various α-actinin–YC-Nanos.** (A) Time course of changes in F_{yellow}/F_{cyan} during spontaneous beating in myocytes expressing α-actinin–YC-Nano15, α-actinin–YC-Nano50, α-actinin–YC-Nano65, or α-actinin–YC-Nano140 in the Z disks. n = 4–12 cells. For strong possible fluorescence signal recordings, measurements were performed in 2.0 mM Ca^{2+}-HEPES–Tyrode's solution at 37°C. See Video 2. (B) Maximal (R_{max}) and minimal (R_0) FRET signals for α-actinin–YC-Nano15, α-actinin–YC-Nano50, α-actinin–YC-Nano65, and α-actinin–YC-Nano140 expressed in the Z disks of myocytes during spontaneous beating (data obtained for 5 s as in A). Closed symbols, R_0; open symbols, R_{max}. (C) Values of ΔR (i.e., $R_{max} - R_0$) for α-actinin–YC-Nanos. Data obtained from A and B. No significant differences were observed between groups (Tukey-Kramer test). (D) Values of the ratio of ΔR to R_0 (i.e., $\Delta R/R_0$) for α-actinin–YC-Nanos. **, P < 0.01; and ***, P < 0.001 compared with α-actinin-YC-Nano140 (Tukey-Kramer test). Note that in D, $\Delta R/R_0$ was highest for α-actinin–YC-Nano140, followed by α-actinin–YC-Nano65, α-actinin–YC-Nano50, and α-actinin–YC-nano15, suggesting that among the α-actinin–YC-Nano complexes tested, α-actinin–YC-Nano140 is most sensitive to a change in local $[Ca^{2+}]_i$ at Z disks in cardiomyocytes, and hence it is the most ideal for the simultaneous investigation of local Ca^{2+} dynamics and SL displacement. Bars in each graph indicate mean values.

indicator (compare Shintani et al., 2014), as a reference. We found that the time course of the F_{yellow}/F_{cyan} duration of α-actinin–YC-Nano140 was longer than that of Fluo-4, at both low (i.e., 22°C; ∼2 and ∼1 s for α-actinin–YC-Nano140 and Fluo-4, respectively) and high (i.e., 37°C; ∼1.2 and ∼0.7 s for α-actinin–YC-Nano140 and Fluo-4, respectively) temperatures (Fig. 3 A). In addition, time to peak and decay time were both significantly longer for α-actinin–YC-Nano140 than Fluo-4 at both temperatures (Fig. 3, B and C).

Here, we discuss possible mechanisms regarding the slow kinetics of α-actinin–YC-Nano140 in response to a change in local $[Ca^{2+}]_i$, as compared with that of Fluo-4. Although Fluo-4 emits fluorescence upon Ca^{2+} binding, the increase in the FRET signal of YC-Nano140, i.e., an increase in F_{yellow} and a decrease in F_{cyan}, occurs after Ca^{2+} binding to CaM and the ensuing conformational changes within the molecular complex (Fig. 1 B). Indeed, it has been reported that the k_{on} and k_{off} values vary markedly between YC-Nano140 and Fluo-3 (i.e., k_{on}: ∼2.4 and ∼80 $\mu M^{-1}s^{-1}$ for YC-Nano140 and Fluo-3, respectively; k_{off}: ∼0.3 and ∼90 s^{-1} for YC-Nano140 and Fluo-3, respectively; compare Table S1; Shirokova et al., 1996; Horikawa et al., 2010). Therefore, it is reasonably understood that the present findings on the differential kinetics between YC-Nano140 and Fluo-4 underlie predominantly the varying chemical nature of the molecules. A similar result has been reported on various genetically encoded Ca^{2+} indicators (whose molecular conformation changes upon Ca^{2+} binding to CaM) that shows a longer time course of CaT than that obtained with the small molecule Ca^{2+} indicator Fura-2 (see Kaestner et al. [2014] for details).

Interestingly, an increase in temperature from 22°C to 37°C abbreviated time to peak as well as decay time, with a greater magnitude for α-actinin–YC-Nano140 in both parameters; namely, the magnitudes of abbreviation in time to peak and decay time were ∼45% (∼30%) and ∼55% (∼40%), respectively, for α-actinin–YC-Nano140 (Fluo-4; Fig. 3, B and C). A general rule of protein physics tells us that conformational changes of a protein–protein complex are decelerated (accelerated) as the temperature is decreased (increased), owing to reduced (enhanced) thermal fluctuation in solution. Therefore, the present findings appear to support the interpretation that the time required for con-

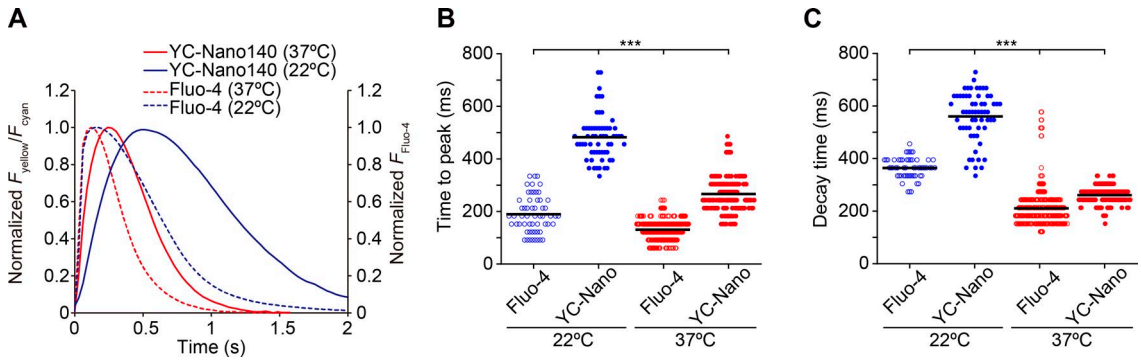

Figure 3. **Comparison of a time course of CaT detected by α-actinin–YC-Nano140 with that by Fluo-4 in cardiomyocytes at different temperatures during spontaneous beating.** (A) Time course of a change in F_{yellow}/F_{cyan} (α-actinin–YC-Nano140) or Fluo-4 fluorescence in cardiomyocytes at 22°C and 37°C. CaT was normalized at the peak for all curves. Each curve was averaged from five beats obtained in 8–24 cells (see B for experimental numbers). (B) Graph comparing the time to peak values for α-actinin–YC-Nano140 or Fluo-4 at 22°C and 37°C. *n* = 57 beats (8 cells), 61 beats (8 cells), 514 beats (24 cells), and 203 beats (14 cells) for Fluo-4 (22°C), α-actinin–YC-Nano140 (22°C), Fluo-4 (37°C), and α-actinin–YC-Nano140 (37°C), respectively. (C) Graph comparing the decay time values for α-actinin–YC-Nano140 and Fluo-4 at 22°C and 37°C. *n*, same as in B. (B and C) ***, P < 0.001 (Tukey-Kramer test). Bars in each graph indicate mean values.

formational change of α-actinin–YC-Nano140 underlies its relatively slow kinetics.

An increase in temperature enhances Ca^{2+} influx through sarcolemmal Ca^{2+} channels in cardiomyocytes (see Allen [1996] and references therein). Therefore, in the experiments with Fluo-4, the abbreviation of time to peak (i.e., by ∼30%) upon an increase in temperature from 22°C to 37°C is likely caused by an increase in Ca^{2+} influx through sarcolemmal Ca^{2+} channels. Likewise, the abbreviation of decay time (i.e., by ∼40%) is likely caused by a well-established increase in the ATP-dependent SR Ca^{2+} pump activity (see Bers [2001] and references therein).

Next, we analyzed the time course of changes in F_{yellow}/F_{cyan} and SL at different temperatures (i.e., 22°C and 37°C; Fig. 4, A and B). As in the case for F_{yellow}/F_{cyan} (see above), time to peak for SL change became abbreviated upon an increase in temperature (Fig. 4 C), indicating enhanced actomyosin interaction (see Bers [2001] and references therein). The magnitude of abbreviation was greater for SL (∼60%) than F_{yellow}/F_{cyan} (∼45%; Fig. 4 C), suggesting that because sarcomere shortening simply reflects actomyosin interaction (with ATPase), it is more sensitive to a change in temperature (as in Bers, 2001) than a rise in F_{yellow}/F_{cyan} (which may be uncoupled with an ATPase reaction, e.g., Ca^{2+} influx through sarcolemmal Ca^{2+} channels; see discussion above). We found that the peak of SL shortening preceded that of F_{yellow}/F_{cyan} at both temperatures, with the difference (noted as "delay time" in Fig. 4 D) significantly larger at 37°C (92 ± 53 ms) than at 22°C (31 ± 50 ms). Given these findings, one may point out that the relative slow response of α-actinin–YC-Nano140 to Ca^{2+} may be a disadvantage in the analysis of cardiac EC coupling, despite its beneficial capability of the simultaneous analysis of local Ca^{2+} and SL displacement via expression at a particular region in a cell. We consider that this issue will be technically solved by calculation. As generally known, the k_{off} and k_{on} values of the currently available Ca^{2+} indicators of any type (including Fluo-4) are too slow to obtain physiologically relevant changes in CaT (or Ca^{2+} sparks) in cardiomyocytes. Therefore, in order to accurately quantify the dynamics of $[Ca^{2+}]_i$, occurring either locally or globally, or both, in cardiomyocytes, the fluorescence signals of α-actinin–YC-Nano140 need to be calibrated to true signals, based on the temperature-dependent values of its k_{on} and k_{off} (as demonstrated by others on adult ventricular myocytes; Kaestner et al., 2014; Shang et al., 2014). See Supplemental discussion III and Fig. S4.

The relatively slow kinetics of α-actinin–YC-Nano140 may limit its use as a Ca^{2+} sensor at high stimulation frequencies. Accordingly, we investigated whether α-actinin–YC-Nano140 enables simultaneous measurement of local $[Ca^{2+}]_i$ and sarcomere dynamics at a physiologically relevant stimulation frequency, as performed in our previous study by using AcGFP expression in the Z disks (i.e., ∼240 beats per min [∼4 Hz] for rat neonates; Smotherman et al., 1991). Consistent with the findings of our previous studies on adult (Serizawa et al., 2011) as well as on neonatal (Shintani et al., 2014) myocytes of the rat, diastolic F_{yellow}/F_{cyan} was elevated by ∼0.7 U upon electric stimulation, with a relatively minor influence on systolic F_{yellow}/F_{cyan} (Fig. 5 A and Video 3). Approximately 2 s after the onset of electric stimulation, stable SL changes with a magnitude of ∼0.06 µm appeared and continued until the cessation of stimulation. We found that as observed during spontaneous beating (Figs. 1 and 4), SL decreased (increased) in response to a rise (fall) in F_{yellow}/F_{cyan} during the stimulation period (systolic and diastolic SLs, ∼1.80 and ∼1.86 µm, respectively;

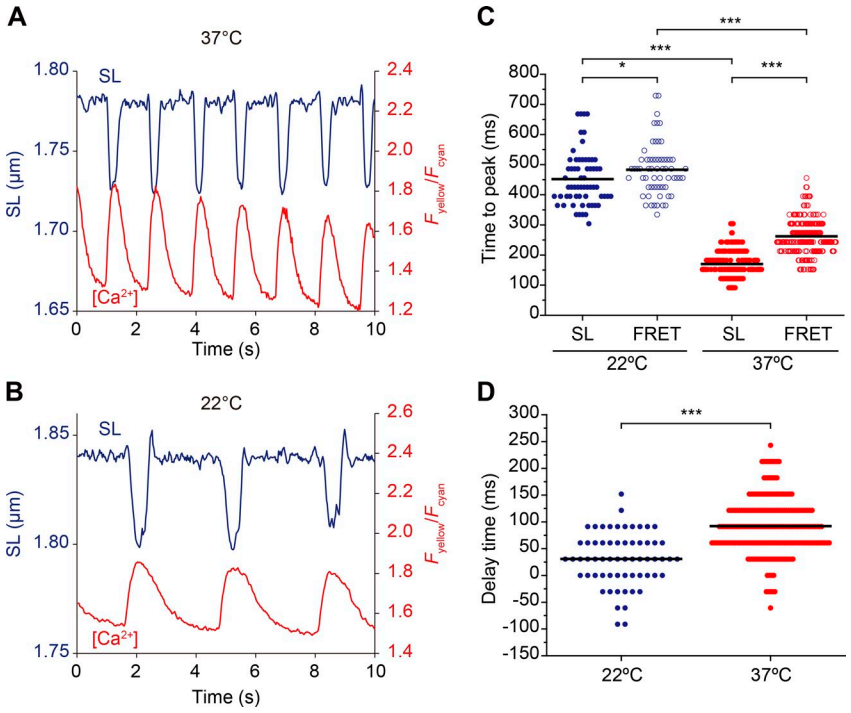

Figure 4. **Changes in SL and local [Ca^{2+}] during spontaneous beating at different temperatures.** (A) Time course of changes in SL and local F_{yellow}/F_{cyan} measured with α-actinin–YC-Nano140 during spontaneous beating at 37°C. Data were averaged from 10 sarcomeres. (B) Same as in A at 22°C. Data were averaged from 13 sarcomeres. (C) Graph summarizing time to peak values of changes in SL and F_{yellow}/F_{cyan} at 22°C and 37°C. *, $P < 0.05$; and ***, $P < 0.001$ (Tukey-Kramer test). (D) Graph comparing delay time (difference in time between SL and F_{yellow}/F_{cyan}) at 22°C and 37°C. ***, $P < 0.001$ (Mann-Whitney *U* test). Bars in each graph indicate mean values.

Fig. 5 B). Our FFT analyses revealed that a single peak existed at 5 Hz for both SL and F_{yellow}/F_{cyan} (Fig. 5 C), though the magnitude of the change in F_{yellow}/F_{cyan} during electrical stimulation was smaller than that during spontaneous beating. Although the rate of rise or fall of $[Ca^{2+}]_i$ becomes reportedly faster in cardiomyocytes during the course of development (Haddock et al., 1999), the present experimental findings suggest that the expression of YC-Nano140 in the Z disks is a useful tool for analyzing EC coupling at the single sarcomere level at physiologically relevant action potential frequencies in myocytes, as well as in vivo by incorporating α-actinin–YC-Nano140 into adenoviruses (see Kobirumaki-Shimozawa et al., 2016). See Supplemental discussion IV and Fig. S5.

Because α-actinin–YC-Nano140 allows us to analyze not only sarcomere dynamics but also local $[Ca^{2+}]_i$ changes, we then investigated the effects of β-adrenergic stimulation (50 nM ISO) on EC coupling at the single sarcomere level. A multitude of data showed a tendency of an increase in the frequency of spontaneous beating upon application of ISO; i.e., 33 ± 6 and 47 ± 23 bpm ($P > 0.05$) in the absence and presence of ISO, respectively (Fig. 6 A). We then converted the parameters and constructed a relationship of F_{yellow}/F_{cyan} versus SL and found that the relationship showed a

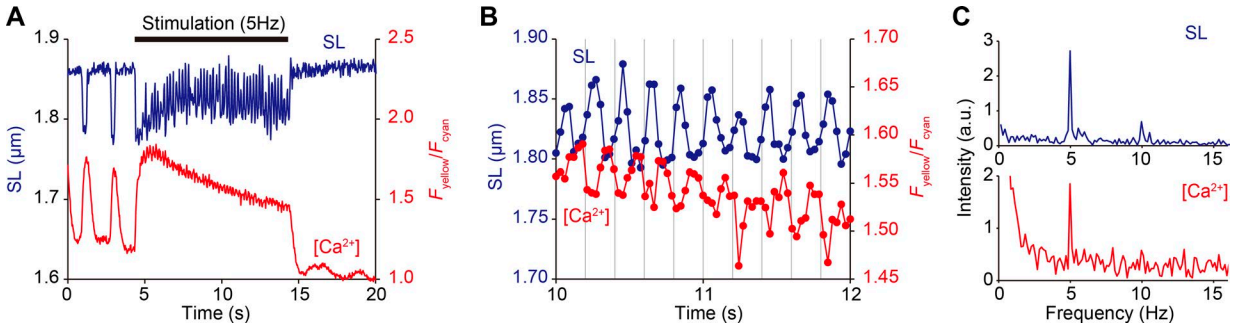

Figure 5. **Simultaneous imaging of local $[Ca^{2+}]_i$ and SL upon electrical stimulation at 5 Hz.** (A) Time course of changes in F_{yellow}/F_{cyan} (red) and SL (blue) in a cardiomyocyte. Electrical stimulation was performed for 10 s (from 5 to 15 s on the x axis). Bar, period for electrical stimulation. See Video 3. (B) Enlarged view of the graph showing time-dependent changes in F_{yellow}/F_{cyan} and SL in A from 10 to 12 s. Note that SL changes in a reciprocal manner in response to a change in F_{yellow}/F_{cyan} (as previously demonstrated by us using Fluo-4: see Shintani et al., 2014). (C, top) FFT analysis for the change in SL. (bottom) Same as in the top, for the change in F_{yellow}/F_{cyan}. Note that only one peak is present at 5 Hz for both SL and F_{yellow}/F_{cyan}, indicating that the EC coupling (i.e., an increase in local $[Ca^{2+}]_i$ and the ensuing actomyosin interaction) occurs locally at the single sarcomere level under the present condition. Data were averaged from four individual sarcomeres for both F_{yellow}/F_{cyan} and SL.

counter-clockwise ellipsoidal trajectory (long and short axes in the x and y directions, respectively) in the absence and presence of ISO (as reported by Butler et al. [2015] in isolated canine ventricular myocytes; Fig. 6 B).

ISO significantly increased systolic F_{yellow}/F_{cyan} from ∼2.3 to ∼2.4 U (Fig. 6 C), showing enhanced CaT in local regions of myocytes where imaging was conducted. Likewise, diastolic F_{yellow}/F_{cyan} was increased by a similar magnitude as systolic F_{yellow}/F_{cyan} (i.e., ∼10%; Fig. 6 C). It should be pointed out that given the range of systolic F_{yellow}/F_{cyan} (up to ∼3.2; Fig. 6 A), Ca^{2+} binding to the CaM domain of YC-Nano140 was not saturated in the presence of ISO because the application of 1 µM Iono markedly increased the value to the range of ∼4.8 to ∼6.6 (Fig. S3). Although the increase in systolic F_{yellow}/F_{cyan} was in line with the findings of a previous study (e.g., Zou et al., 2001), i.e., coupled primarily with enhanced Ca^{2+} release from the SR, the increase in diastolic F_{yellow}/F_{cyan} was rather unexpected (because the enhanced SR Ca^{2+} pump activity via phospholamban [PLN] phosphorylation would decrease the resting $[Ca^{2+}]_i$ level; Bers, 2001). In a well-organized study, Morimoto et al. (2009) demonstrated that β-adrenergic stimulation causes a leak of Ca^{2+} from RyR of the SR, coupled presumably with an increase in open probability of RyR via PKA-dependent phosphorylation. We consider that a similar mechanism operates in neonatal cardiomyocytes, as well as in adult cardiomyocytes (Morimoto et al., 2009; Prosser et al., 2010), resulting in a decrease in $\Delta R/R_0$ upon application of ISO (Fig. 6 D; cf. Zou et al., 2001; despite similar values of ΔR, i.e., 0.72 ± 0.17 and 0.72 ± 0.18, respectively, in the absence and presence of ISO; $P > 0.05$). Because absolute SL values (Fig. 6 E) and ΔSL (i.e., magnitude of SL change from diastole to systole; Fig. 6 F) were not significantly affected by β-adrenergic stimulation, the apparent null effect of ISO on ΔSL may be a compensatory mechanism to protect the immaturely developed intracellular morphology of neonatal cardiomyocytes (see Di Maio et al. [2007] and references therein) from possible hypercontracture.

It is important that although ISO did not significantly affect absolute SL values in both diastole and systole, it affected the dynamics of sarcomeric contractions, showing a significant increase in shortening velocity (Fig. 6 G), as well as in lengthening velocity (Fig. 6 H). Likewise, ISO reduced the time to peak values for both F_{yellow}/F_{cyan} and SL (Fig. 6 I), and shortened the F_{yellow}/F_{cyan} decay time (Fig. 6 J). We consider these effects to be based on the following molecular mechanisms: (a) the reduction in the time to peak for F_{yellow}/F_{cyan} is caused by enhanced Ca^{2+} release from RyR of the SR via increasing Ca^{2+} entry through PKA-based phosphorylation of L-type Ca^{2+} channels, and (b) the shortening of the decay time is coupled with acceleration of Ca^{2+} uptake into the SR via an increase in the Ca^{2+} ATPase caused by PLN phosphorylation.

It is well established that enhanced relaxation upon β-adrenergic stimulation results from both Ca^{2+}-dependent and -independent mechanisms, both of which are coupled with the activation of PKA; the former mechanism is via phosphorylation of PLN (and the ensuing acceleration of Ca^{2+} uptake into the SR), and the latter is via phosphorylation of troponin I (TnI; and the ensuing Ca^{2+} dissociation from troponin C [hence, enhanced cross-bridge detachment]). In fetal/neonatal cardiomyocytes, slow skeletal TnI (which does not have PKA-dependent phosphorylation sites) is expressed, in place of cardiac TnI (Martin et al., 1991). It is therefore unlikely that in the present study PKA-dependent phosphorylation of TnI underlies enhanced relaxation. Instead, accumulating evidence indicates that PKA-dependent phosphorylation of myosin-binding protein C promotes relaxation via acceleration of cross-bridge kinetics (e.g., Stelzer et al., 2007; Tong et al., 2008; Previs et al., 2015; Rosas et al., 2015). Accordingly, the present findings on the effects of β-adrenergic stimulation are consistent with the notion that acceleration of relaxation (or lengthening) of sarcomeres in neonates, upon β-adrenergic stimulation, predominantly underlies PKA-dependent phosphorylation of PLN and myosin-binding protein C.

Previously, we demonstrated via α-actinin–AcGFP expression in cardiomyocytes that the averaging of SL along myofibrils causes marked underestimation of the magnitude of SL displacement as the result of superpositioning of shortening/lengthening of individual sarcomeres at different timings (Shintani et al., 2014), highlighting the powerfulness of SL nanometry in the analysis of sarcomere dynamics. In the present study, by fully taking advantage of the nature of α-actinin–YC-Nano140, in that it enables simultaneous imaging of SL dynamics and CaT at the single sarcomere level, we investigated the effects of pharmacological perturbations on EC coupling at the single sarcomere level.

First, we analyzed individual behaviors of sequentially connecting single sarcomeres along a myofibril, simultaneously with local CaT. Although the magnitude of shortening or lengthening of sequentially connecting eight sarcomeres varied from ∼0.1 to ∼0.2 µm (with diastolic SL varying from ∼1.65 to ∼1.92 µm) during the course of contraction, the averaged SL displacement became diminished to the level of ∼0.06 µm (Fig. 7 A and Video 4). In contrast to sarcomere dynamics, the changes in F_{yellow}/F_{cyan} in the Z disks were well synchronized, suggesting that CaT occurs in a uniform manner along a myofibril, but each sarcomere exerts its own pattern of shortening/lengthening during spontaneous beating (as in Shintani et al., 2014). Therefore, the imbalance of tug of war between sarcomeres along a myofibril (because of the individuality of each sarcomere,

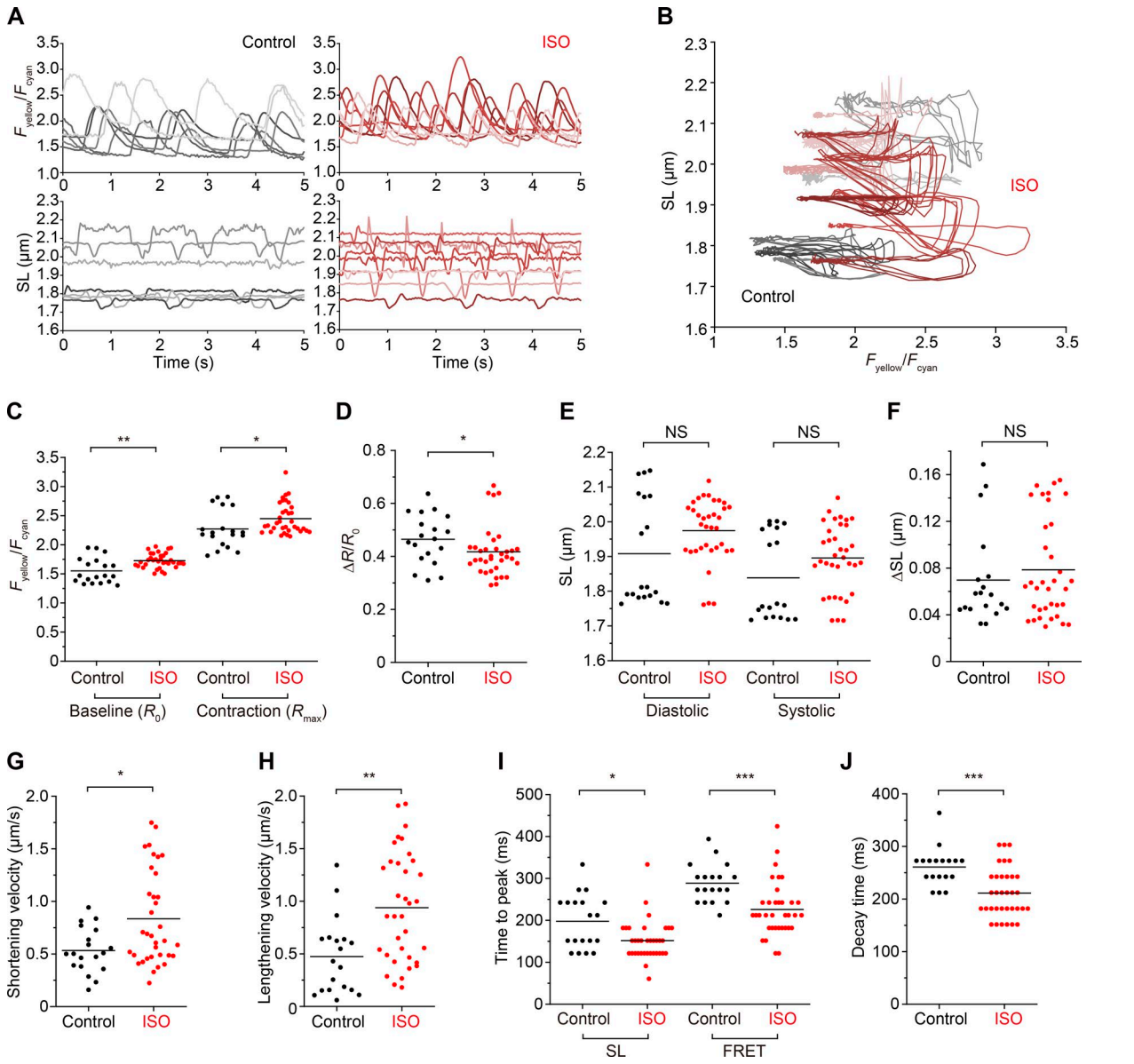

Figure 6. **Effects of ISO on local coupling of $[Ca^{2+}]_i$ and SL dynamics.** (A) Individual data showing time courses of changes in F_{yellow}/F_{cyan} (top) and SL (bottom) in α-actinin–YC-Nano140–expressing cardiomyocytes during spontaneous beating in the absence (left; indicated as "control") and presence (right) of 50 nM ISO. n = 7 and 9 in the absence and presence of ISO, respectively. Experiments were performed at 37°C. (B) Individual data showing the relationship of F_{yellow}/F_{cyan} versus SL in the absence and presence of ISO. A closed loop-like trajectory was observed, regardless of the use of ISO (compare Butler et al., 2015). (C) Comparison of F_{yellow}/F_{cyan} values during relaxation (R_0) and contraction (R_{max}) in the absence and presence of ISO. F_{yellow}/F_{cyan} was significantly higher for both R_0 and R_{max}. (D) Comparison of $\Delta R/R_0$ in the absence and presence of ISO (see Fig. 2 for $\Delta R/R_0$). (E) SL values in the absence and presence of ISO, during relaxation and contraction. ISO did not significantly affect SL, regardless of the contractile state. (F) ΔSL (difference between SL at relaxation and contraction) values in the absence and presence of ISO. No significant difference was observed between groups. Likewise, the variance was similar for both groups (i.e., from ∼0.03 to ∼0.17 μm for control [difference, ∼0.14 μm] and from ∼0.03 to ∼0.15 μm for ISO [difference, ∼0.12 μm]). (G) Shortening velocity of SL dynamics in the absence and presence of ISO. The velocity became significantly faster in the presence of ISO. (H) Lengthening velocity of SL dynamics in the absence and presence of ISO. (I) Time to peak values for changes in F_{yellow}/F_{cyan} and SL in the absence and presence of ISO. The values were less for both parameters, indicating the acceleration of the EC coupling at the single sarcomere level. (J) Comparison of the decay time for F_{yellow}/F_{cyan}. The time was shorter in the presence of ISO, indicating enhanced removal of cytosolic $[Ca^{2+}]_i$, presumably via acceleration of SR Ca^{2+} pump coupled with PLN phosphorylation (see Bers [2001] and references therein). In all graphs, horizontal bars indicate mean values. *, P < 0.05; **, P < 0.01; and ***, P < 0.001 (Mann-Whitney U test).

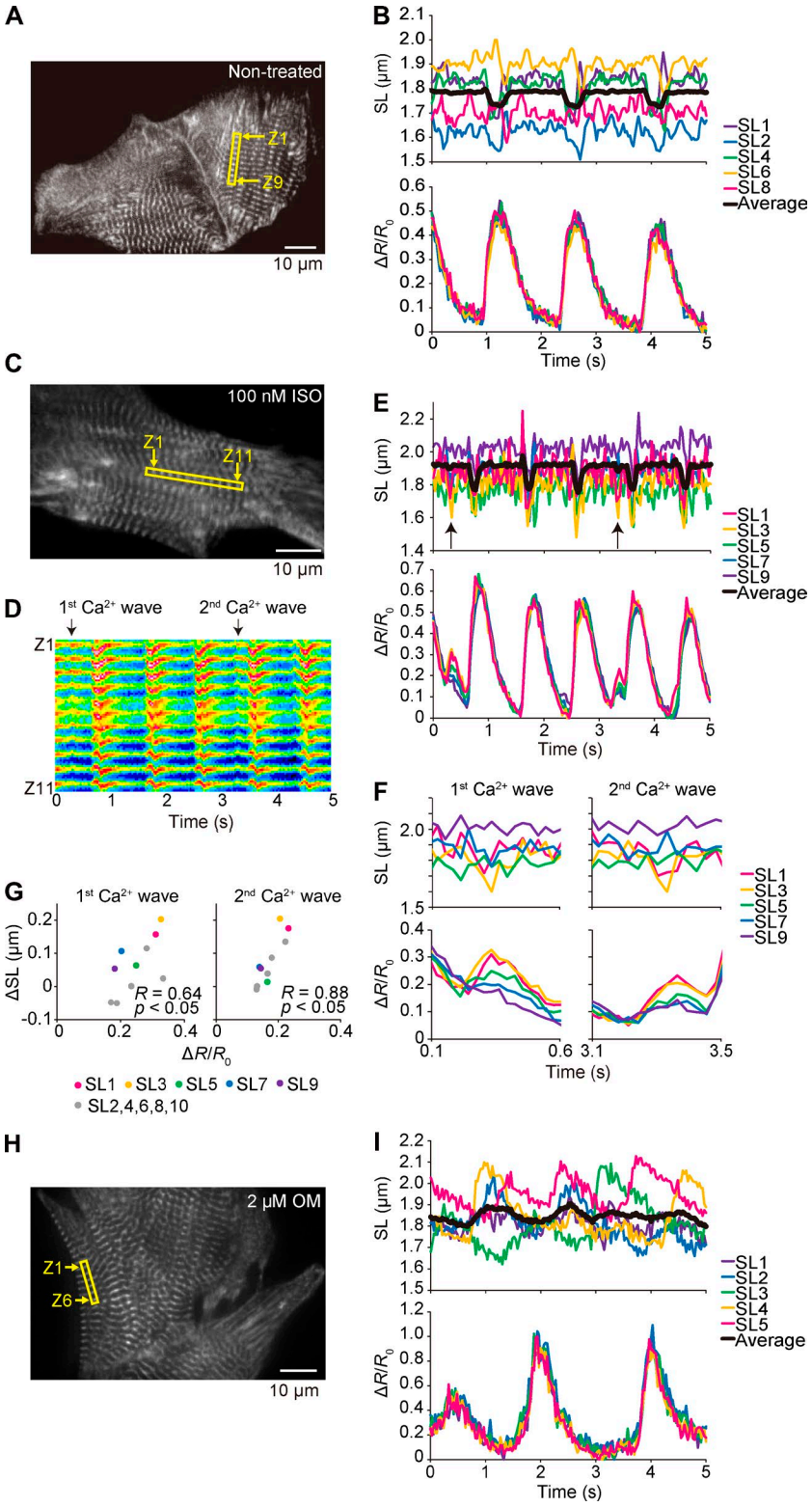

Figure 7. **Sarcomere dynamics and local $[Ca^{2+}]_i$ along a myofibril in a cardiomyocyte under various conditions.** (A) Epi-illumination image of a myocyte expressing α-actinin–YC-Nano140. Sarcomeres in the yellow rectangular region were used for the analyses on F_{yellow}/F_{cyan} and SL dynamics (Z1 and Z9, numbers of the Z disks for analyzed sarcomeres). Experiments were performed at 37°C. (B, top) Time course of changes in the lengths of five sarcomeres in a myocyte in A during spontaneous beating. Black line, superimposed data of sequentially connecting eight sarcomeres. (bottom) Time course of changes in the mean F_{yellow}/F_{cyan} of the Z disks of each sarcomere. See Video 4. (C) Same as in A, but the experimentation was performed in the presence of 100 nM ISO. Sarcomeres in the yellow rectangular region in the epi-illumination image were used for the analyses on F_{yellow}/F_{cyan} and SL dynamics (Z1 and Z11, numbers of the Z disks for analyzed sarcomeres). (D) As indicated in this kymograph of the yellow fluorescence signal (for 5 s), two major Ca^{2+} waves were observed during the course of imaging. (E) Time courses (5 s) of changes in SL and $\Delta R/R_0$. Arrows indicate the points at which Ca^{2+} waves (and the ensuing sarcomere contractions) occurred. (F) Time course (0.5 s) of changes in SL and Ca^{2+} waves. (G) Variances in SL versus $\Delta R/R_0$, resulting in the significant linear correlation between $\Delta R/R_0$ and ΔSL for both the first and second Ca^{2+} waves. See Video 5. (H) Same as in A, but the experimentation was performed in the presence of 2 μM OM. Epi-illumination image of a myocyte expressing α-actinin–YC-Nano140. Sarcomeres in the yellow rectangular region were used for the analyses on F_{yellow}/F_{cyan} and SL dynamics (Z1 and Z6, numbers of the Z disks for analyzed sarcomeres). Experiments were performed at 36°C. (I, top) Time course of changes in the lengths of sequentially connecting five sarcomeres in a myocyte in H during spontaneous beating. Black line, superimposed data. (bottom) Time course of changes in the mean F_{yellow}/F_{cyan} of the Z disks of each sarcomere. See Video 6.

such as variance in structure or PKA or protein kinase C–dependent phosphorylation of thick/thin filaments and the ensuing difference in Ca^{2+} sensitivity), but not varying levels of local $[Ca^{2+}]_i$, is likely to underlie unsynchronized sarcomeric behaviors. In a recent study on the beating heart in healthy adult mice, we demonstrated that SL in left ventricular myocytes varied by as much as ∼300 nm in both diastole and systole (Kobirumaki-Shimozawa et al., 2016). Therefore, future studies should be directed to elucidating how individual dynamic properties of cardiac sarcomeres are integrated to exert rhythmic pump functions of the heart by sys-

tematically analyzing local EC coupling in myocytes at various locations of the heart.

We then performed experiments in the presence of 100 nM ISO. As noted in Fig. 6, ISO exhibited a tendency of an increase in the beating frequency (Fig. 7, C–E). It is of interest that as previously demonstrated by others (Gómez et al., 1996; Ogrodnik and Niggli, 2010; Santiago et al., 2013), ISO caused increases in local $[Ca^{2+}]_i$, resulting in irregular sarcomeric contractions (see Video 5 and a kymograph in Fig. 7 D). A significant correlation between $\Delta R/\Delta R_0$ and ΔSL showed that the sarcomeric contractions were indeed triggered by the local Ca^{2+} waves (Fig. 7, F and G). Interestingly, a distinct variance in the magnitude of Ca^{2+} waves was seen (as well as in the amplitude of the ensuing sarcomeric oscillations; e.g., both greater for sarcomeres #1 and #3 compared with sarcomeres #5, #7, and #9). This finding suggests that the variance in the magnitude of enhanced Ca^{2+} release from the SR coupled with PKA-based PLN phosphorylation along a myofibril underlies the sarcomeric contractions. Because the Ca^{2+} wave–induced local SL shortening is considerable with a magnitude of up to ∼0.2 µm (Fig. 7 G), these local sarcomeric contractions, albeit occurring locally, may disorganize rhythmic contractions of cardiomyocytes per se in the beating heart in vivo. These Ca^{2+} waves, therefore, may play a role in arrhythmogenesis (Prosser et al., 2010) and warrant future investigations in vivo (as in Kobirumaki-Shimozawa et al., 2016).

We previously demonstrated that the amplitude of actomyosin-based, sarcomeric auto-oscillations (i.e., cell-SPOCs that occur under steady intermediate activation conditions at pCa ∼6.0; see Ishiwata et al., 2011; Kobirumaki-Shimozawa et al., 2014; and references therein) was increased upon application of the actomyosin activator OM (0.6 µM). In the present study, under the condition of spontaneous beating, sarcomeric oscillations composed of quick lengthening followed by slow shortening (i.e., indistinguishable from cell-SPOCs; see Shintani et al. [2014] and references therein) were observed upon application of 2 µM OM, along a myofibril, of which oscillations were not synchronized with CaT (Fig. 7, H and I; and Video 6). In a series of previous studies, we demonstrated that SPOCs occur in myocytes with or without membrane solubilization treatment by using a detergent (such as Triton X-100), as long as two types of cross-bridges, i.e., attached and detached cross-bridges, are present in the sarcomere over threshold populations (see Ishiwata et al., 2011; Shintani et al., 2014; and references therein), with the amplitude growing and frequency slowing as the force along a myofibril increases. Given the pharmacological action of OM that enhances myosin binding to thin filaments (Malik et al., 2011), the present finding with OM (Fig. 7 I) suggests that SPOCs can occur and, more importantly, exhibit a distinct rhythm in living myocytes in association with an increase in load along myofibrils under partial activation states. We therefore consider that an elevated concentration of OM may disrupt the coupling between Ca^{2+} and myofibrillar contractility (as demonstrated by the irregular pattern of SL changes in Fig. 7 I) and set a Ca^{2+}-independent, actomyosin-based rhythm of overall myocyte contraction.

Collectively, α-actinin–YC-Nano140 allowed for quantitative analyses of coupling/decoupling between sarcomere dynamics and $[Ca^{2+}]_i$ at the single sarcomere level along a myofibril in living neonatal myocytes, with or without pharmacological perturbation.

In conclusion, we developed an experimental system with neonatal cardiomyocytes that facilitates nano-imaging of sarcomeric dynamic properties, simultaneously with local $[Ca^{2+}]_i$. The present system has the potential to visualize how EC coupling begins to fail at the onset of ischemia or the initial stage of hypertrophic or dilated cardiomyopathy, at the subcellular space where the T tubules invaginate and associate with the Z disks, thereby providing useful information to elucidate the pathogenesis of various heart diseases. Therefore, future studies should be directed toward quantifying the means by which single sarcomere cardiac EC coupling changes in health and disease during the course of development.

ACKNOWLEDGMENTS

We thank Dr. Kazuki Horikawa for his generous donation of various YC-Nano cDNAs. We also thank Ms. Naoko Tomizawa (The Jikei University School of Medicine) for technical assistance.

This work was supported in part by Ministry of Education, Culture, Sports, Science and Technology of Japan Grants-in-Aid for Scientific Research (B) (to N. Fukuda: 15H04677), Challenging Exploratory Research (to N. Fukuda: 26560225; and to F. Kobirumaki-Shimozawa: 15K12524), and Scientific Research on Innovative Areas (to N. Fukuda: 23107003) and the Japan Society for the Promotion of Science (JSPS) Fellows (to K. Oyama: 15J10205). K. Oyama and S.A. Shintani are research fellows of JSPS. This study was also supported in part by the Japan Heart Foundation (to F. Kobirumaki-Shimozawa).

The authors declare no competing financial interests.

Richard L. Moss served as editor.

Submitted: 8 April 2016

Accepted: 23 August 2016

REFERENCES

Allen, T.J. 1996. Temperature dependence of macroscopic L-type calcium channel currents in single guinea pig ventricular myocytes. *J. Cardiovasc. Electrophysiol.* 7:307–321. http://dx.doi.org/10.1111/j.1540-8167.1996.tb00532.x

Allen, D.G., and J.C. Kentish. 1985. The cellular basis of the length-tension relation in cardiac muscle. *J. Mol. Cell. Cardiol.* 17:821–840. http://dx.doi.org/10.1016/S0022-2828(85)80097-3

Asahi, M., K. Otsu, H. Nakayama, S. Hikoso, T. Takeda, A.O. Gramolini, M.G. Trivieri, G.Y. Oudit, T. Morita, Y. Kusakari, et al. 2004. Cardiac-specific overexpression of sarcolipin inhibits sarco(endo)plasmic reticulum Ca^{2+} ATPase (SERCA2a) activity

and impairs cardiac function in mice. *Proc. Natl. Acad. Sci. USA*. 101:9199–9204. http://dx.doi.org/10.1073/pnas.0402596101

Bers, D.M. 2001. Excitation-contraction coupling and cardiac contractile force. Developments in Cardiovascular Medicine. Vol. 237. Kluwer Academic Publishers, Dordrecht, Netherlands. 427 pp.

Bers, D.M. 2002. Cardiac excitation-contraction coupling. *Nature*. 415:198–205. http://dx.doi.org/10.1038/415198a

Butler, L., C. Cros, K.L. Oldman, A.R. Harmer, A. Pointon, C.E. Pollard, and N. Abi-Gerges. 2015. Enhanced characterization of contractility in cardiomyocytes during early drug safety assessment. *Toxicol. Sci.* 145:396–406. http://dx.doi.org/10.1093/toxsci/kfv062

Colella, M., F. Grisan, V. Robert, J.D. Turner, A.P. Thomas, and T. Pozzan. 2008. Ca^{2+} oscillation frequency decoding in cardiac cell hypertrophy: role of calcineurin/NFAT as Ca^{2+} signal integrators. *Proc. Natl. Acad. Sci. USA*. 105:2859–2864. http://dx.doi.org/10.1073/pnas.0712316105

Di Maio, A., K. Karko, R.M. Snopko, R. Mejía-Alvarez, and C. Franzini-Armstrong. 2007. T-tubule formation in cardiacmyocytes: two possible mechanisms? *J. Muscle Res. Cell Motil.* 28:231–241. http://dx.doi.org/10.1007/s10974-007-9121-x

Fukuda, N., J. O-Uchi, D. Sasaki, H. Kajiwara, S. Ishiwata, and S. Kurihara. 2001. Acidosis or inorganic phosphate enhances the length dependence of tension in rat skinned cardiac muscle. *J. Physiol.* 536:153–160. http://dx.doi.org/10.1111/j.1469-7793.2001.00153.x

Fukuda, N., T. Terui, S. Ishiwata, and S. Kurihara. 2010. Titin-based regulations of diastolic and systolic functions of mammalian cardiac muscle. *J. Mol. Cell. Cardiol.* 48:876–881. http://dx.doi.org/10.1016/j.yjmcc.2009.11.013

Gómez, A.M., H. Cheng, W.J. Lederer, and D.M. Bers. 1996. Ca^{2+} diffusion and sarcoplasmic reticulum transport both contribute to $[Ca^{2+}]_i$ decline during Ca^{2+} sparks in rat ventricular myocytes. *J. Physiol.* 496:575–581. http://dx.doi.org/10.1113/jphysiol.1996.sp021708

González, A., W.G. Kirsch, N. Shirokova, G. Pizarro, G. Brum, I.N. Pessah, M.D. Stern, H. Cheng, and E. Ríos. 2000. Involvement of multiple intracellular release channels in calcium sparks of skeletal muscle. *Proc. Natl. Acad. Sci. USA*. 97:4380–4385. http://dx.doi.org/10.1073/pnas.070056497

Haddock, P.S., W.A. Coetzee, E. Cho, L. Porter, H. Katoh, D.M. Bers, M.S. Jafri, and M. Artman. 1999. Subcellular $[Ca^{2+}]_i$ gradients during excitation-contraction coupling in newborn rabbit ventricular myocytes. *Circ. Res.* 85:415–427. http://dx.doi.org/10.1161/01.RES.85.5.415

Hanft, L.M., F.S. Korte, and K.S. McDonald. 2008. Cardiac function and modulation of sarcomeric function by length. *Cardiovasc. Res.* 77:627–636. http://dx.doi.org/10.1093/cvr/cvm099

Hollingworth, S., C. Soeller, S.M. Baylor, and M.B. Cannell. 2000. Sarcomeric Ca^{2+} gradients during activation of frog skeletal muscle fibres imaged with confocal and two-photon microscopy. *J. Physiol.* 526:551–560. http://dx.doi.org/10.1111/j.1469-7793.2000.t01-1-00551.x

Horikawa, K., Y. Yamada, T. Matsuda, K. Kobayashi, M. Hashimoto, T. Matsu-ura, A. Miyawaki, T. Michikawa, K. Mikoshiba, and T. Nagai. 2010. Spontaneous network activity visualized by ultrasensitive Ca^{2+} indicators, yellow Cameleon-Nano. *Nat. Methods*. 7:729–732. http://dx.doi.org/10.1038/nmeth.1488

Ishiwata, S., Y. Shimamoto, and N. Fukuda. 2011. Contractile system of muscle as an auto-oscillator. *Prog. Biophys. Mol. Biol.* 105:187–198. http://dx.doi.org/10.1016/j.pbiomolbio.2010.11.009

Jacot, J.G., A.D. McCulloch, and J.H. Omens. 2008. Substrate stiffness affects the functional maturation of neonatal rat ventricular myocytes. *Biophys. J.* 95:3479–3487. http://dx.doi.org/10.1529/biophysj.107.124545

Jacot, J.G., H. Kita-Matsuo, K.A. Wei, H.S. Chen, J.H. Omens, M. Mercola, and A.D. McCulloch. 2010. Cardiac myocyte force development during differentiation and maturation. *Ann. N. Y. Acad. Sci.* 1188:121–127. http://dx.doi.org/10.1111/j.1749-6632.2009.05091.x

Kaestner, L., A. Scholz, Q. Tian, S. Ruppenthal, W. Tabellion, K. Wiesen, H.A. Katus, O.J. Müller, M.I. Kotlikoff, and P. Lipp. 2014. Genetically encoded Ca^{2+} indicators in cardiac myocytes. *Circ. Res.* 114:1623–1639. http://dx.doi.org/10.1161/CIRCRESAHA.114.303475

Katz, A.M. 2002. Ernest Henry Starling, his predecessors, and the "Law of the Heart". *Circulation*. 106:2986–2992. http://dx.doi.org/10.1161/01.CIR.0000040594.96123.55

Kobirumaki-Shimozawa, F., T. Inoue, S.A. Shintani, K. Oyama, T. Terui, S. Minamisawa, S. Ishiwata, and N. Fukuda. 2014. Cardiac thin filament regulation and the Frank-Starling mechanism. *J. Physiol. Sci.* 64:221–232. http://dx.doi.org/10.1007/s12576-014-0314-y

Kobirumaki-Shimozawa, F., K. Oyama, T. Shimozawa, A. Mizuno, T. Ohki, T. Terui, S. Minamisawa, S. Ishiwata, and N. Fukuda. 2016. Nano-imaging of the beating mouse heart in vivo: Importance of sarcomere dynamics, as opposed to sarcomere length per se, in the regulation of cardiac function. *J. Gen. Physiol.* 147:53–62. http://dx.doi.org/10.1085/jgp.201511484

Malik, F.I., J.J. Hartman, K.A. Elias, B.P. Morgan, H. Rodriguez, K. Brejc, R.L. Anderson, S.H. Sueoka, K.H. Lee, J.T. Finer, et al. 2011. Cardiac myosin activation: a potential therapeutic approach for systolic heart failure. *Science*. 331:1439–1443. http://dx.doi.org/10.1126/science.1200113

Martin, A.F., K. Ball, L.Z. Gao, P. Kumar, and R.J. Solaro. 1991. Identification and functional significance of troponin I isoforms in neonatal rat heart myofibrils. *Circ. Res.* 69:1244–1252. http://dx.doi.org/10.1161/01.RES.69.5.1244

Miyawaki, A., J. Llopis, R. Heim, J.M. McCaffery, J.A. Adams, M. Ikura, and R.Y. Tsien. 1997. Fluorescent indicators for Ca^{2+} based on green fluorescent proteins and calmodulin. *Nature*. 388:882–887. http://dx.doi.org/10.1038/42264

Miyawaki, A., O. Griesbeck, R. Heim, and R.Y. Tsien. 1999. Dynamic and quantitative Ca^{2+} measurements using improved cameleons. *Proc. Natl. Acad. Sci. USA*. 96:2135–2140. http://dx.doi.org/10.1073/pnas.96.5.2135

Morimoto, S., J. O-Uchi, M. Kawai, T. Hoshina, Y. Kusakari, K. Komukai, H. Sasaki, K. Hongo, and S. Kurihara. 2009. Protein kinase A-dependent phosphorylation of ryanodine receptors increases Ca^{2+} leak in mouse heart. *Biochem. Biophys. Res. Commun.* 390:87–92. http://dx.doi.org/10.1016/j.bbrc.2009.09.071

Ogrodnik, J., and E. Niggli. 2010. Increased Ca^{2+} leak and spatiotemporal coherence of Ca^{2+} release in cardiomyocytes during β-adrenergic stimulation. *J. Physiol.* 588:225–242. http://dx.doi.org/10.1113/jphysiol.2009.181800

Previs, M.J., B.L. Prosser, J.Y. Mun, S.B. Previs, J. Gulick, K. Lee, J. Robbins, R. Craig, W.J. Lederer, and D.M. Warshaw. 2015. Myosin-binding protein C corrects an intrinsic inhomogeneity in cardiac excitation-contraction coupling. *Sci. Adv.* 1:e1400205. http://dx.doi.org/10.1126/sciadv.1400205

Prosser, B.L., C.W. Ward, and W.J. Lederer. 2010. Subcellular Ca^{2+} signaling in the heart: the role of ryanodine receptor sensitivity. *J. Gen. Physiol.* 136:135–142. http://dx.doi.org/10.1085/jgp.201010406

Ríos, E., M.D. Stern, A. González, G. Pizarro, and N. Shirokova. 1999. Calcium release flux underlying Ca^{2+} sparks of frog skeletal muscle. *J. Gen. Physiol.* 114:31–48. http://dx.doi.org/10.1085/jgp.114.1.31

Rodriguez, A.G., S.J. Han, M. Regnier, and N.J. Sniadecki. 2011. Substrate stiffness increases twitch power of neonatal cardiomyocytes in correlation with changes in myofibril structure and intracellular calcium. *Biophys. J.* 101:2455–2464. http://dx.doi.org/10.1016/j.bpj.2011.09.057

Rosas, P.C., Y. Liu, M.I. Abdalla, C.M. Thomas, D.T. Kidwell, G.F. Dusio, D. Mukhopadhyay, R. Kumar, K.M. Baker, B.M. Mitchell, et al. 2015. Phosphorylation of cardiac Myosin-binding protein-C is a critical mediator of diastolic function. *Circ Heart Fail.* 8:582–594. http://dx.doi.org/10.1161/CIRCHEARTFAILURE.114.001550

Santiago, D.J., E. Ríos, and T.R. Shannon. 2013. Isoproterenol increases the fraction of spark-dependent RyR-mediated leak in ventricular myocytes. *Biophys. J.* 104:976–985. http://dx.doi.org/10.1016/j.bpj.2013.01.026

Serizawa, T., T. Terui, T. Kagemoto, A. Mizuno, T. Shimozawa, F. Kobirumaki, S. Ishiwata, S. Kurihara, and N. Fukuda. 2011. Real-time measurement of the length of a single sarcomere in rat ventricular myocytes: a novel analysis with quantum dots. *Am. J. Physiol. Cell Physiol.* 301:C1116–C1127. http://dx.doi.org/10.1152/ajpcell.00161.2011

Shang, W., F. Lu, T. Sun, J. Xu, L.-L. Li, Y. Wang, G. Wang, L. Chen, X. Wang, M.B. Cannell, et al. 2014. Imaging Ca^{2+} nanosparks in heart with a new targeted biosensor. *Circ. Res.* 114:412–420. http://dx.doi.org/10.1161/CIRCRESAHA.114.302938

Shintani, S.A., K. Oyama, F. Kobirumaki-Shimozawa, T. Ohki, S. Ishiwata, and N. Fukuda. 2014. Sarcomere length nanometry in rat neonatal cardiomyocytes expressed with α-actinin–AcGFP in Z discs. *J. Gen. Physiol.* 143:513–524. http://dx.doi.org/10.1085/jgp.201311118

Shintani, S.A., K. Oyama, N. Fukuda, and S. Ishiwata. 2015. High-frequency sarcomeric auto-oscillations induced by heating in living neonatal cardiomyocytes of the rat. *Biochem. Biophys. Res. Commun.* 457:165–170. http://dx.doi.org/10.1016/j.bbrc.2014.12.077

Shirokova, N., J. García, G. Pizarro, and E. Ríos. 1996. Ca^{2+} release from the sarcoplasmic reticulum compared in amphibian and mammalian skeletal muscle. *J. Gen. Physiol.* 107:1–18. http://dx.doi.org/10.1085/jgp.107.1.1

Smotherman, W.P., S.R. Robinson, A.E. Ronca, J.R. Alberts, and P.G. Hepper. 1991. Heart rate response of the rat fetus and neonate to a chemosensory stimulus. *Physiol. Behav.* 50:47–52. http://dx.doi.org/10.1016/0031-9384(91)90496-B

Stelzer, J.E., J.R. Patel, J.W. Walker, and R.L. Moss. 2007. Differential roles of cardiac myosin-binding protein C and cardiac troponin I in the myofibrillar force responses to protein kinase A phosphorylation. *Circ. Res.* 101:503–511. http://dx.doi.org/10.1161/CIRCRESAHA.107.153650

Tallini, Y.N., M. Ohkura, B.R. Choi, G. Ji, K. Imoto, R. Doran, J. Lee, P. Plan, J. Wilson, H.B. Xin, et al. 2006. Imaging cellular signals in the heart in vivo: Cardiac expression of the high-signal Ca^{2+} indicator GCaMP2. *Proc. Natl. Acad. Sci. USA.* 103:4753–4758. http://dx.doi.org/10.1073/pnas.0509378103

Tanaka, H., M. Oyamada, E. Tsujii, T. Nakajo, and T. Takamatsu. 2002. Excitation-dependent intracellular Ca^{2+} waves at the border zone of the cryo-injured rat heart revealed by real-time confocal microscopy. *J. Mol. Cell. Cardiol.* 34:1501–1512. http://dx.doi.org/10.1006/jmcc.2002.2096

Tong, C.W., J.E. Stelzer, M.L. Greaser, P.A. Powers, and R.L. Moss. 2008. Acceleration of crossbridge kinetics by protein kinase A phosphorylation of cardiac myosin binding protein C modulates cardiac function. *Circ. Res.* 103:974–982. http://dx.doi.org/10.1161/CIRCRESAHA.108.177683

Tsien, R.Y. 1980. New calcium indicators and buffers with high selectivity against magnesium and protons: design, synthesis, and properties of prototype structures. *Biochemistry.* 19:2396–2404. http://dx.doi.org/10.1021/bi00552a018

Tsien, R.Y., T. Pozzan, and T.J. Rink. 1982a. T-cell mitogens cause early changes in cytoplasmic free Ca^{2+} and membrane potential in lymphocytes. *Nature.* 295:68–71. http://dx.doi.org/10.1038/295068a0

Tsien, R.Y., T. Pozzan, and T.J. Rink. 1982b. Calcium homeostasis in intact lymphocytes: cytoplasmic free calcium monitored with a new, intracellularly trapped fluorescent indicator. *J. Cell Biol.* 94:325–334. http://dx.doi.org/10.1083/jcb.94.2.325

Zoghbi, M.E., P. Bolaños, C. Villalba-Galea, A. Marcano, E. Hernández, M. Fill, and A.L. Escobar. 2000. Spatial Ca^{2+} distribution in contracting skeletal and cardiac muscle cells. *Biophys. J.* 78:164–173. http://dx.doi.org/10.1016/S0006-3495(00)76582-9

Zou, Y., A. Yao, W. Zhu, S. Kudoh, Y. Hiroi, M. Shimoyama, H. Uozumi, O. Kohmoto, T. Takahashi, F. Shibasaki, et al. 2001. Isoproterenol activates extracellular signal-regulated protein kinases in cardiomyocytes through calcineurin. *Circulation.* 104:102–108. http://dx.doi.org/10.1161/hc2601.090987